Article

Cell Reports

The RNA-Binding Protein SYNCRIP Is a Component of the Hepatocyte Exosomal Machinery Controlling MicroRNA Sorting

Graphical Abstract

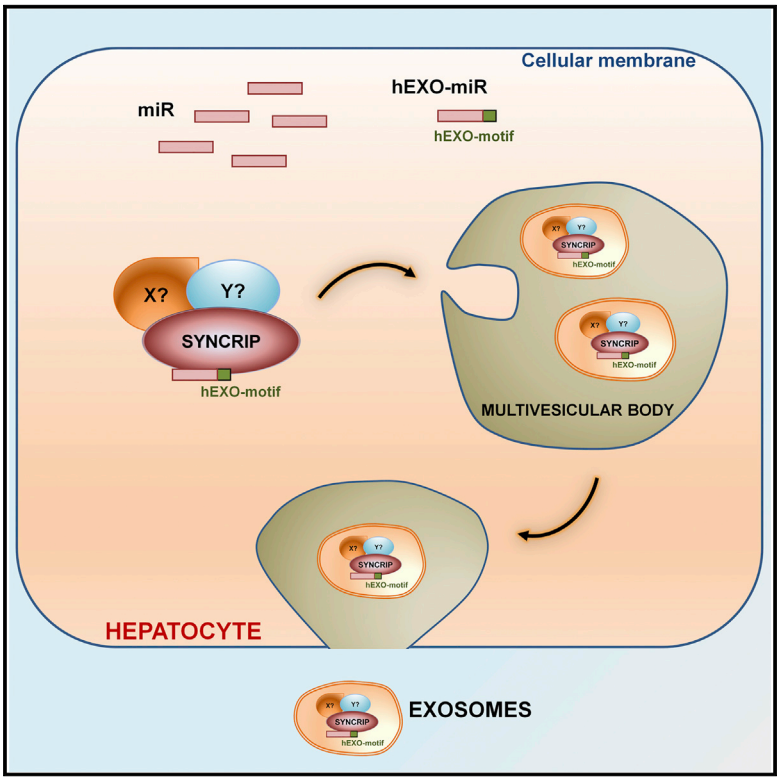

Authors

Laura Santangelo, Giorgio Giurato, Carla Cicchini, ..., Tonino Alonzi, Alessandro Weisz, Marco Tripodi

Correspondence

tripodi@bce.uniroma1.it

In Brief

Santangelo et al. shed light on the mechanism that allows a cell to load exosomes with a specific repertoire of miRNAs, showing a functional role of a specific miRNA motif and a protein that specifically interacts with it, the RNA-binding protein SYNCRIP.

Highlights

- SYNCRIP interacts specifically with selected miRNAs
- SYNCRIP has a functional role in exosomal sorting of specific miRNAs
- A hEXO miRNA extra-seed motif determines exosomal loading

Accession Numbers

E-MTAB-4502

Santangelo et al., 2016, Cell Reports *17*, 799–808
October 11, 2016
http://dx.doi.org/10.1016/j.celrep.2016.09.031

Cell Reports
Article

The RNA-Binding Protein SYNCRIP Is a Component of the Hepatocyte Exosomal Machinery Controlling MicroRNA Sorting

Laura Santangelo,[1,3,4] Giorgio Giurato,[2,4] Carla Cicchini,[1] Claudia Montaldo,[3] Carmine Mancone,[1,3] Roberta Tarallo,[2] Cecilia Battistelli,[1] Tonino Alonzi,[3] Alessandro Weisz,[2] and Marco Tripodi[1,3,5,*]

[1]Department of Cellular Biotechnologies and Haematology, Istituto Pasteur Italia, Fondazione Cenci Bolognetti, Sapienza University of Rome, Viale Regina Elena 324, 00161 Rome, Italy

[2]Laboratory of Molecular Medicine and Genomics, Department of Medicine, Surgery and Dentistry, Schola Medica Salernitana, University of Salerno, Via Salvador Allende 1, 84081 Baronissi, Italy

[3]National Institute for Infectious Diseases L. Spallanzani, IRCCS, Via Portuense 292, 00149 Rome, Italy

[4]Co-first author

[5]Lead Contact

*Correspondence: tripodi@bce.uniroma1.it

http://dx.doi.org/10.1016/j.celrep.2016.09.031

SUMMARY

Despite clear evidence that exosomal microRNAs (miRNAs) are able to modulate the cellular microenvironment and that exosomal RNA cargo selection is deregulated in pathological conditions, the mechanisms controlling specific RNA sorting into extracellular vesicles are still poorly understood. Here, we identified the RNA binding protein SYNCRIP (synaptotagmin-binding cytoplasmic RNA-interacting protein; also known as hnRNP-Q or NSAP1) as a component of the hepatocyte exosomal miRNA sorting machinery. SYNCRIP knockdown impairs sorting of miRNAs in exosomes. Furthermore, SYNCRIP directly binds to specific miRNAs enriched in exosomes sharing a common extra-seed sequence (hEXO motif). The hEXO motif has a role in the regulation of miRNA localization, since embedment of this motif into a poorly exported miRNA enhances its loading into exosomes. This evidence provides insights into the mechanisms of miRNA exosomal sorting process. Moreover, these findings open the way for the possible selective modification of the miRNAs exosomal cargo.

INTRODUCTION

Growing evidence points to extracellular vesicles (EVs) (Skog et al., 2008) as pivotal mediators of cell-cell communication among neighboring or distant cells (Lo Cicero et al., 2015) and in both physiological and pathological processes (Mittelbrunn and Sánchez-Madrid, 2012). EVs comprise two main types of vesicles, either directly originating from the plasma membrane (i.e., microvesicles) or derived from the endosomal compartment, as intraluminal vesicles within multivesicular bodies (MVBs) (i.e., exosomes).

In exosomes, characterized by diameters of 40–100 nm, the specific cargo of proteins, lipids, and RNAs (including mRNAs, microRNAs [miRNAs], and other non-coding RNAs) reflects the specific cells of origin (Vlassov et al., 2012). Moreover, exosomal cargo has been described to change in response to different cellular conditions (Skog et al., 2008). In view of the informational nature of the molecules specifically carried by exosomes, it is crucial to better understand the molecular mechanisms concerning their sorting for export and the selectivity of this process.

Concerning miRNAs, it has been reported that exosome miRNA content does not match the intracellular profile of these molecules, given that a subset of miRNAs appear to preferentially localize to exosomes (Guduric-Fuchs et al., 2012; Mittelbrunn et al., 2011; Nolte-'t Hoen et al., 2012; Ohshima et al., 2010). Notably, miRNAs with oncogenic or inflammatory function have been found to aberrantly increase in extracellular vesicles circulating in patients' body fluids (De Toro et al., 2015; Guo and Guo, 2015; Lo Cicero et al., 2015).

To date, mechanisms controlling the specific loading of miRNAs in exosomes are still largely unknown, and it appears conceivable that several loading mechanisms may govern exosome sorting of specific subsets of miRNAs. Indeed, different pathways and molecules have been described to impact miRNAs sorting in different cell types and tissues (Janas et al., 2015; Villarroya-Beltri et al., 2014; Zhang et al., 2015). With respect to sequence-dependent miRNA sorting, a determinant called the EXO motif, which is able to guide miRNA inclusion in exosomes of human primary T-lymphocytes, has been identified (Villarroya-Beltri et al., 2013). This RNA sequence is recognized by the sumoylated form of the heterogeneous nuclear ribonucleoprotein A2B1 (hnRNPA2B1) that controls miRNAs sorting in exosomes (Villarroya-Beltri et al., 2013). Moreover, a 3′-end nucleotide addition in miRNAs has been shown to impact their selective sorting in B cells (Koppers-Lalic et al., 2014).

Here, we identified, in a hepatocyte in vitro cellular model, molecular players of the pathways for selective miRNA sorting into exosomes. We first observed selective sorting of various classes of RNAs in exosomes, identifying a repertoire of

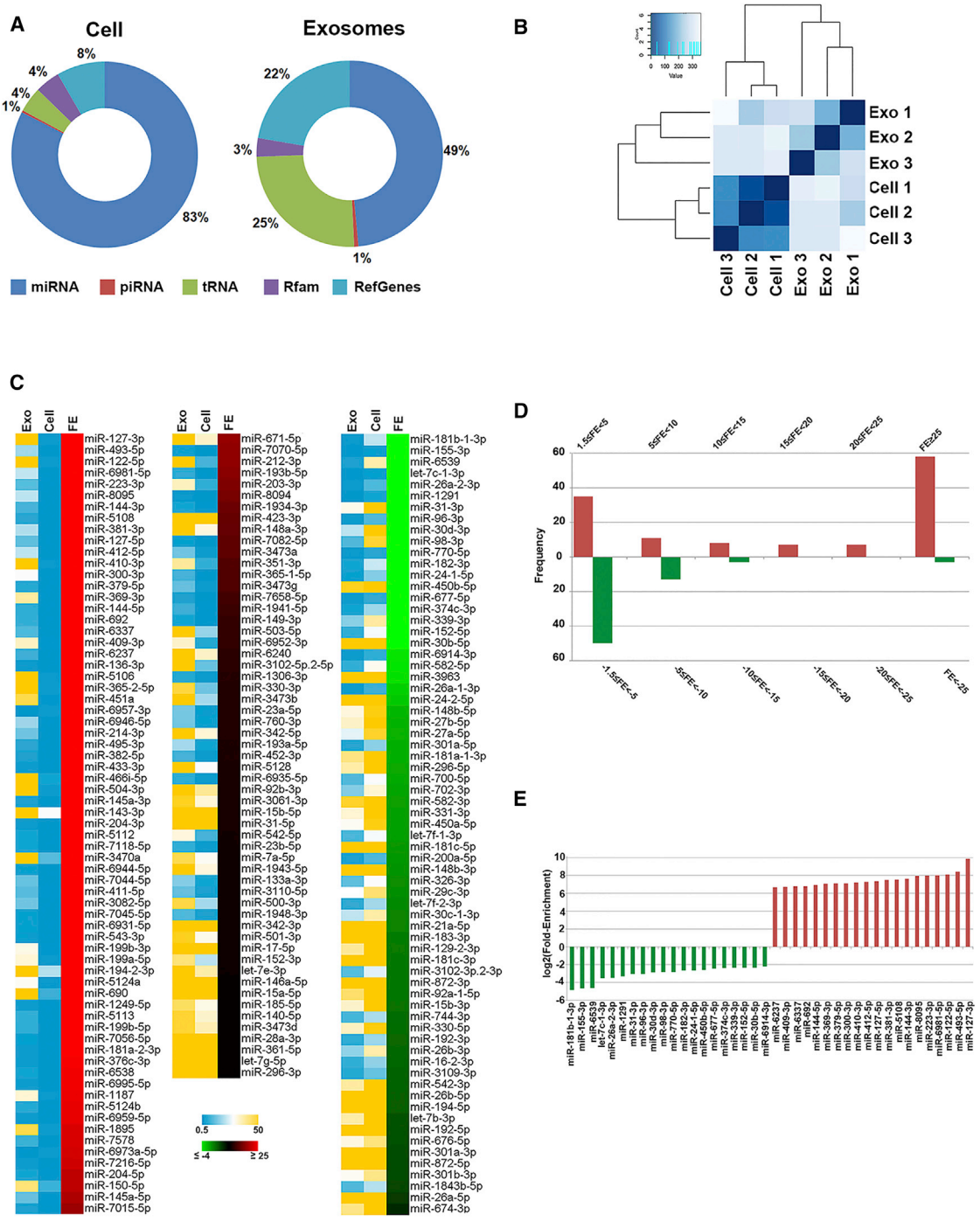

Figure 1. Overview of Intracellular and Exosomal miRNAs Distribution and Identification of a Common Sequence Element at the 3′ End of Preferentially Exported miRNAs

(A) Pie charts showing the percentage of small non-coding RNA species identified in intracellular (left) and exosomal (right) compartments by small RNA-seq, performed on three independent biological replicates. High-quality and adaptor trimmed reads were mapped against miRNA, tRNA, and piRNA sequences, small non-coding RNA sequences included in the Rfam database, and fragments of mature RNA reported in RefGenes (downloaded from the UCSC Browser). The values shown represent the average values of biological replicates.

(B) Sample-to-sample distance heatmap performed on mature miRNAs identified in cells and exosomes in three independent biological replicates. Sample distances were generated using the Poisson distance on raw count matrix values, after exclusion of miRNAs with read counts <3 (first quantile [Q1]).

(legend continued on next page)

exosomal-enriched miRNAs (hEXO-miRNAs). By analyzing by MALDI-TOF/TOF mass spectrometry (MS) the protein interactors specifically binding to two exosome-enriched miRNAs (i.e., miR-3470a and miR-194-2-3p), we identified the synaptotagmin-binding cytoplasmic RNA-interacting protein (SYNCRIP; also known as hnRNP-Q or NSAP1). SYNCRIP functional role in sorting was highlighted: its knockdown impaired the exosomal loading of specific exosome-enriched miRNAs. Moreover, RNA immunoprecipitation (RIP) after UV cross-linking demonstrated that this protein binds directly to some hEXO-miRNAs embedding a short sequence in common (hEXO motif) that was shared by ~60% of exosome-enriched miRNAs. Finally, insertion of this sequence in a normally cell-retained miRNA induced its exosomal export, further suggesting a functional role of this motif in small RNA exosome loading.

RESULTS

Characterization of Hepatocyte Cellular and Exosomal MicroRNA Repertoires

In order to investigate on the molecular machinery controlling exosomal miRNA loading, we first aimed to validate an in vitro cellular model sorting a coherent repertoire of RNA molecules. To this aim, we analyzed the intracellular and exosomal profile of small RNAs in three independent biological replicates of hepatocyte cells. By small RNA sequencing (RNA-seq), different classes of small RNAs were reproducibly found to be compartmentalized in exosomes with respect to intracellular RNAs. Indeed, global profiling identified reads aligning to various classes of small non-coding RNA (sncRNAs), where miRNA reads were the most abundant both in the intracellular and exosomal fractions. In the pie chart shown in Figure 1A, the read distribution among RNA families is computed, considering the average value among the sequencing reads obtained in the three biological replicates. In exosomes, the other enriched classes are represented by tRNAs, fragments of mRNAs, PIWI-interacting-RNAs (piRNAs), and other sncRNAs. These classes are also present within the cell with different distributions. These results are in agreement with analyses performed on exosomes from other cell types (Cha et al., 2015; Huang et al., 2013).

To ascertain the existence of miRNAs differentially secreted in exosomes, we quantified the relative abundance of individual miRNAs with respect to the corresponding intracellular ones (here considering those with an expression level above the first quantile computed considering the distribution level; Table S1). We first applied principal-component analysis (PCA) to determine how the overall miRNA profiles differ between cells and exosomes. The same test was performed computing also the Poisson distance between the biological replicates in both cells and exosomes. Both analyses clearly reveal a considerable and consistent diversity between the two miRNA populations (Figure 1B). Next, we performed a more detailed analysis considering each individual miRNA. Results showed the existence of distinct subsets of miRNAs that are either enriched or diminished in exosomes respect to the cells of origin. In particular, 126 miRNAs were enriched (fold enrichment [FE] $\geq$ 1.5; false discovery rate [FDR] $\leq$ 0.10), and 69 miRNAs were under-represented (FE ≤ -1.5, FDR $\leq$ 0.10) in exosomal with respect to the cellular fraction, highlighting as the miRNA profile in exosomes is reproducibly distinct from that of their parental cells. Figure 1C shows, side by side for comparison, the expression level in reads per million (RPM) (log2 scale) of differentially enriched miRNAs between the two compartments. Figure 1D displays the frequency distribution of miRNAs enriched in exosomes (red) or retained in cell compartments (dark green), considering the FE value. Interestingly, the majority of miRNAs are present in exosomes with a high FE value (FE $\geq$ 25), while those retained in cells are characterized by a low FE value ($-1.5 \leq$ FE ≥ -5). Figure 1E reports the actual data relative to the top 20 exosomal-enriched (hEXO-miRNAs) and intracellular-retained (hCYTO-miRNAs) miRNAs, showing that the former reach between 200-fold and 1,200-fold differences and the latter between 6-fold and 110-fold differences between the two compartments.

Overall, these data show an exosome-specific miRNA profile, thus validating the use of this cellular model for the study of the mechanism(s) of selective sorting of these molecules in exosomes.

SYNCRIP Has a Role in Exosomal Sorting of miRNAs

To shed light on the molecular mechanism controlling exosomal miRNA sorting, and in particular to identify protein players, cellular extracts were incubated with streptavidin beads coated with two biotinylated highly exosome-enriched miRNAs (i.e., miR-3470a and miR-194-2-3p), and pulled-down proteins were then subjected to high-throughput identification by MS. As a control, non-coated beads and beads coated with poly(G) RNA were used. Among the RNA-binding proteins precipitated with miRNAs, but not with negative controls (Table S2), we focused on SYNCRIP (Mourelatos et al., 2001) for three reasons: (1) western blot analysis validated that SYNCRIP binds specifically to the hEXO-miRNAs miR-3470a and miR-194-2-3p and not to hCYTO-miR miR-29b or random sequences (Figure 2A), (2) it was described to have a sequence/structure discriminatory capacity and relevant functions in RNA transport (Liu et al., 2009; Svitkin et al., 2013), and (3) it was previously annotated in the major exosome database (http://exocarta.org/gene_summary?gene_id=10492; Keerthikumar et al., 2016)

First, the presence of SYNCRIP in hepatocyte exosomes was confirmed by size-exclusion chromatography (SEC), where it was found to cofractionate with the exosome markers Alix and Tsg101 (Figure 2B) and to be protected from proteinase K digestion (Figure S1A).

Possible contamination by the fetal bovine serum (FBS) used in cell culture was also ruled out, showing that bovine SYNCRYP

(C) Heatmaps showing expression values, expressed as reads per million (RPM; yellow-blue), and fold enrichment (FE; green-red) of mature miRNAs in exosomes (hEXO-miRNAs) versus cells (hCYTO-miRNAs). Only miRNAs with |FE| $\geq$ 1.5 and FDR $\leq$ 0.10 were considered to be differentially enriched. See also Table S1.
(D) Histograms showing the FE value frequency distribution of mature miRNAs that are exported (red columns) into exosomes (hEXO-miRNAs) or retained (green columns) in the cells (hCYTO-miRNAs). miRNAs have been divided into six subgroups based on FE values.
(E) A list of the top 20 cell-retained (hCYTO-miRNAs, green) and exosome-enriched (hEXO-miRNAs, red) miRNAs.

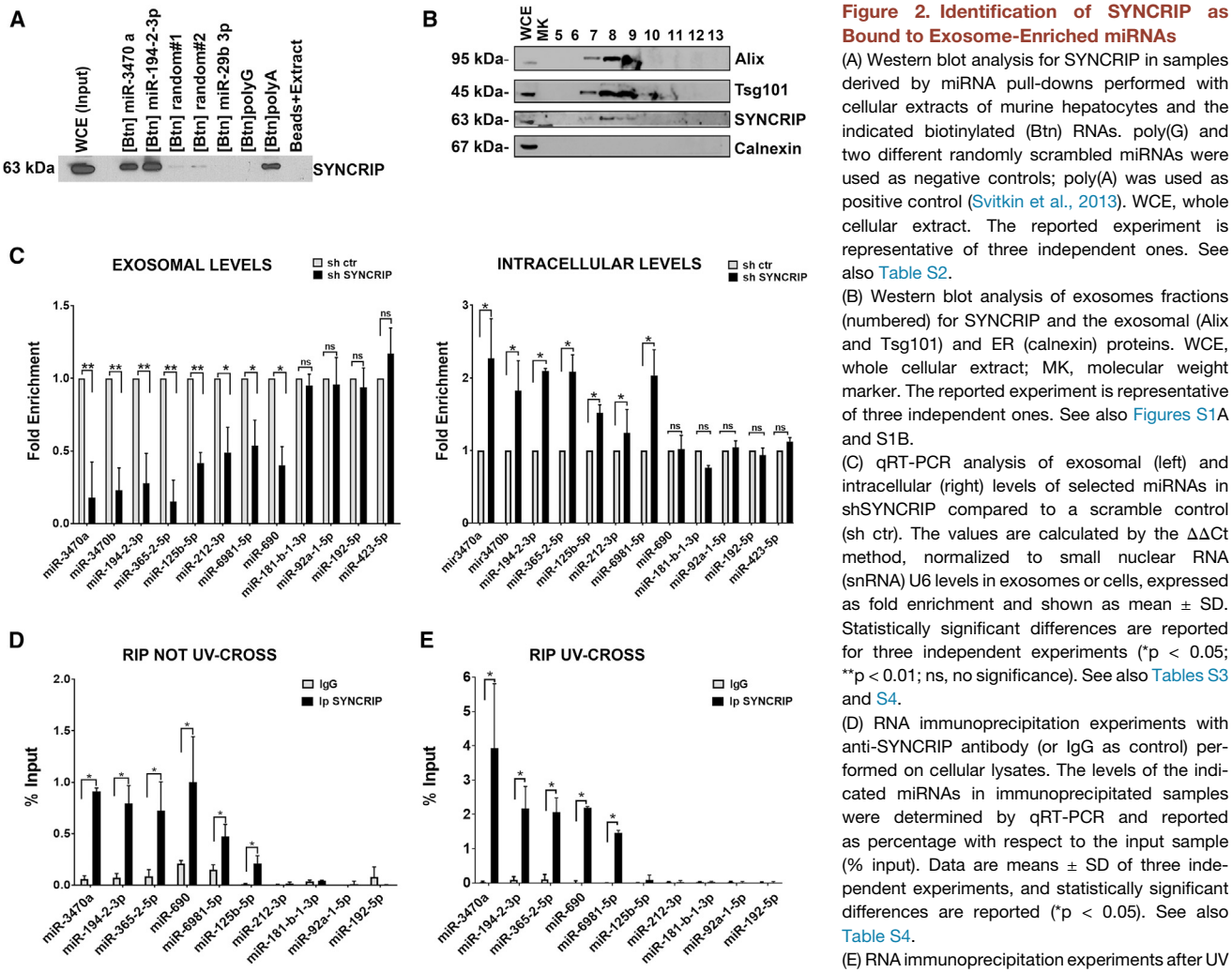

Figure 2. Identification of SYNCRIP as Bound to Exosome-Enriched miRNAs

(A) Western blot analysis for SYNCRIP in samples derived by miRNA pull-downs performed with cellular extracts of murine hepatocytes and the indicated biotinylated (Btn) RNAs. poly(G) and two different randomly scrambled miRNAs were used as negative controls; poly(A) was used as positive control (Svitkin et al., 2013). WCE, whole cellular extract. The reported experiment is representative of three independent ones. See also Table S2.

(B) Western blot analysis of exosomes fractions (numbered) for SYNCRIP and the exosomal (Alix and Tsg101) and ER (calnexin) proteins. WCE, whole cellular extract; MK, molecular weight marker. The reported experiment is representative of three independent ones. See also Figures S1A and S1B.

(C) qRT-PCR analysis of exosomal (left) and intracellular (right) levels of selected miRNAs in shSYNCRIP compared to a scramble control (sh ctr). The values are calculated by the ΔΔCt method, normalized to small nuclear RNA (snRNA) U6 levels in exosomes or cells, expressed as fold enrichment and shown as mean ± SD. Statistically significant differences are reported for three independent experiments (*$p < 0.05$; **$p < 0.01$; ns, no significance). See also Tables S3 and S4.

(D) RNA immunoprecipitation experiments with anti-SYNCRIP antibody (or IgG as control) performed on cellular lysates. The levels of the indicated miRNAs in immunoprecipitated samples were determined by qRT-PCR and reported as percentage with respect to the input sample (% input). Data are means ± SD of three independent experiments, and statistically significant differences are reported (*$p < 0.05$). See also Table S4.

(E) RNA immunoprecipitation experiments after UV cross-linking with anti-SYNCRIP antibody (or IgG as control) performed on cellular lysates. The levels of the indicated miRNAs in immunoprecipitates were determined by qRT-PCR and reported as percentage with respect to the input sample (% input). Data are means ± SD of three independent experiments, and statistically significant differences are reported (*$p < 0.05$). See also Table S4.

was not recognized by the antibody used in all our experiments (Figure S1B). Next, in order to investigate the possible functional role of SYNCRIP in exosomal miRNA loading, the effect of its silencing was assessed. To this aim, we infected hepatocytes with retroviruses expressing different short hairpin RNAs (shRNAs) against SYNCRIP and a scrambled sequence as control. Western blot analysis demonstrated that SYNCRIP levels were significantly reduced in cells infected with the retrovirus targeting SYNCRIP (Figure S2A). qRT-PCR analysis validated as, once SYNCRIP was interfered, a number of the previously characterized hEXO-miRNAs was significantly less represented in the exosome compartment and, notably, their levels were increased in the cell (Figure 2C). RNA-seq analysis of two replicates highlighted as the stable knockdown of SYNCRIP caused significant alterations in enrichment of several exosomal miRNAs (Table S3). Next, to correlate this observation to biochemical evidence, RIPs followed by RT-PCR were performed. The experiments were carried out by using two different approaches: (1) non-denaturing wash protocol, allowing the retrieval of both directly and indirectly bound interactors; and (2) denaturing wash protocol after (UV) cross-linking, allowing the identification of protein-RNA interactions only when direct (indirect interactions are disrupted, according to McHugh et al., 2015 and Battistelli et al., 2016; see Experimental Procedures).

In non-denaturing conditions, the potential binding of seven hEXO-miRNAs modulated by SYNCRIP silencing was assessed: the RIP assays demonstrated that SYNCRIP interacts with miR-3470a, miR-194-2-3p, miR-365-2-5p, miR-6981-5p, miR-690, and miR-125b-5p, but not, interestingly, with miR-212-3p (Figure 2D); the RIP assays performed in denaturing conditions highlighted that miR-3470a, miR-194-2-3p, miR-365-2-5p, miR-6981-5p, and miR-690 interact directly with SYNCRIP (Figure 2E); the cell-retained miRNAs miR-192-5p (although highly abundant in hepatocytes), miR-92a-1-5p, and miR-181b-1 3p were not detected in both of these conditions (Figures 2D and 2E).

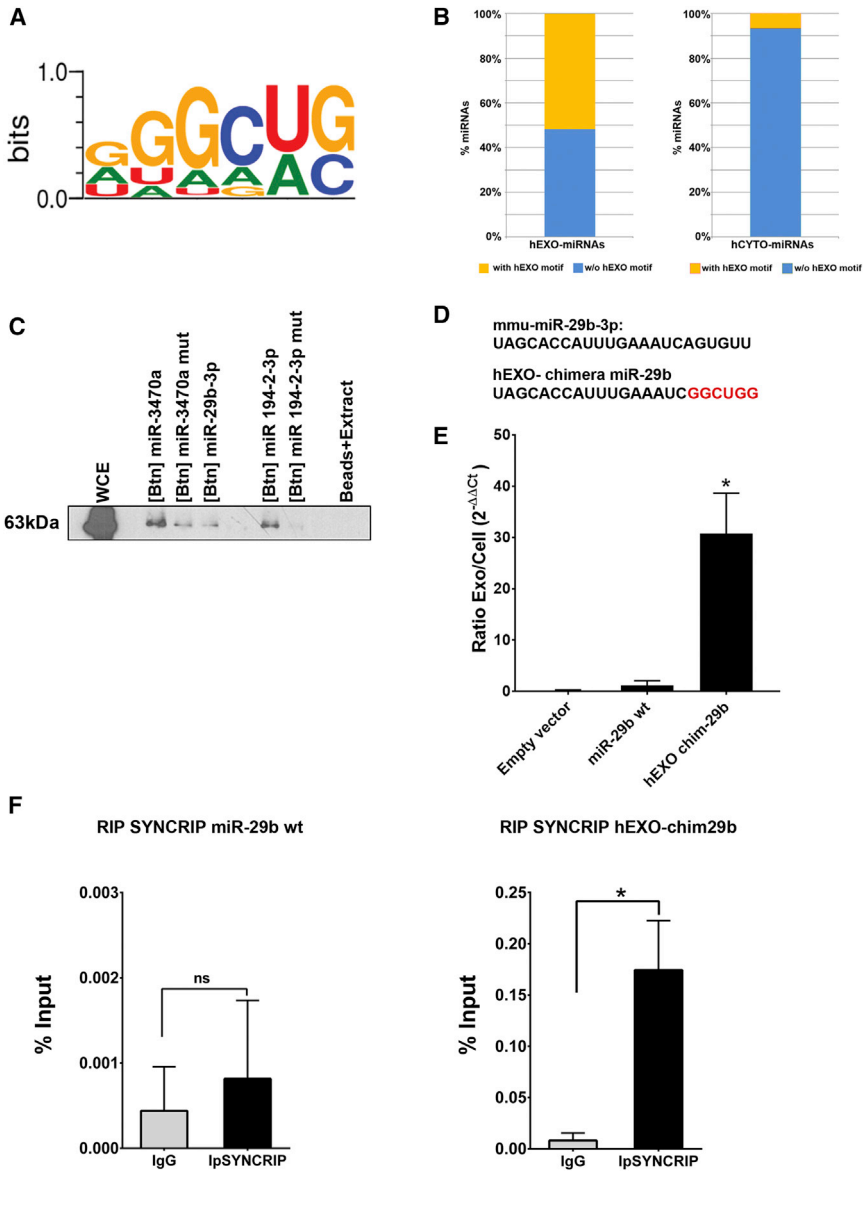

Figure 3. Identification and Functional Characterization of hEXO Motif

(A) The hEXO motif as determined from a bioinformatics comparative analysis performed on exosome-enriched miRNAs. The core GGCU shows high information content (i.e., matrix exhibits high conservation, with ci-value > 60 at this position). The base pair (in capital letters) denotes the core sequence identified by MatDefine (Genomatix). See also Table S5.

(B) Histogram showing the percentage of miRNAs with and without the hEXO motif for both hEXO miRNAs (FE $\geq$ 1.5 and p value $\leq$ 0.05) and hCYTO miRNAs (FE ≤ -1.5 and pvalue $\leq$ 0.05). The GGCU core motif identified with Improbizer in hEXO miRNAs was searched in hCYTO-miRNAs using MatInspector, using a matrix similarity > 0.75. Results show that the GGCU hEXO-motif core is present in 102 out of 170 enriched miRNAs and in 4 out of 108 retained miRNAs.

(C) Western blot analysis for SYNCRIP in samples derived from miRNA pull-downs performed with cellular extracts of murine hepatocytes and the indicated biotinylated (Btn) miRNAs. miR 3470a mut and 194-2-3p mut bear a scrambled hEXO motif (see Table S6). WCE, whole cellular extract. The reported experiment is representative of three independent ones.

(D) Sequences of miR-29b-3p and chimeric miRNA-29b embedding the 3′ end of the exosome: highly enriched and SYNCRIP-binding mir3470a (in red).

(E) qRT-PCR analysis of intracellular and exosomal levels of miR-29b-3p and hEXO-29b chimera (both overexpressed by lentiviral transduction; as a control, an empty vector has been used). Results are reported as fold expression levels of overexpressed WT miR-29b or hEXO-miR-29b chimera versus endogenous levels of miR-29b, each normalized to snRNAU6 levels in exosomes or cells and shown as mean ± SD. Statistically significant differences are reported (*p < 0.05) for three independent experiments.

(F) RIP assays with rabbit polyclonal anti-SYNCRIP and pre-immune IgG (as control) on murine hepatocyte cell extracts. miR-29b-3p and hEXO-29b chimera levels in immunoprecipitated samples were determined by qRT-PCR and reported as percentage with respect to the input sample (% input). Data are means ± SD of three independent experiments, and statistically significant differences are reported (*p < 0.05).

Overall, these analyses demonstrated that SYNCRIP appears to influence the exosomal compartmentalization of several miRNAs, and some of them were shown to directly bind to this protein.

A Subset of miRNAs Enriched in Exosomes Contains a Common Sequence Motif Endowed with a Functional Capacity

Interestingly, sequence comparison of the miRNAs identified as directly bound to SYNCRIP (miR-3470a, miR-194-2-3p, miR-6981-5p, miR-690, and miR-365-2-5p; Figure 2E) highlighted as they share the common short sequence GGCU (see sequences in Table S4).

Therefore, aiming to investigate if this GGCU sequence (Figure 3A) could be differentially present in hEXO-miRNAs with respect to intracellular miRNAs, we performed an unbiased search for over-represented sequence motifs. This analysis by Improbizer (Ao et al., 2004) identified a conserved minimal GGCU motif, hereafter named hEXO, in 64 of exosomal miRNAs (with FE $\geq$ 1.5 and p value $\leq$ 0.05); interestingly, this sequence was preferentially localized in the 3′ region of miRNA (i.e., extra-seed sequence; Table S5). It should be noted, however, that GGCU sequence does not appear to be an exclusive feature of exosome-enriched miRNAs, given that it was found also in 4 out of 108 miRNAs that we classified among the cell retained. The results were further confirmed with MatDefine (Cartharius

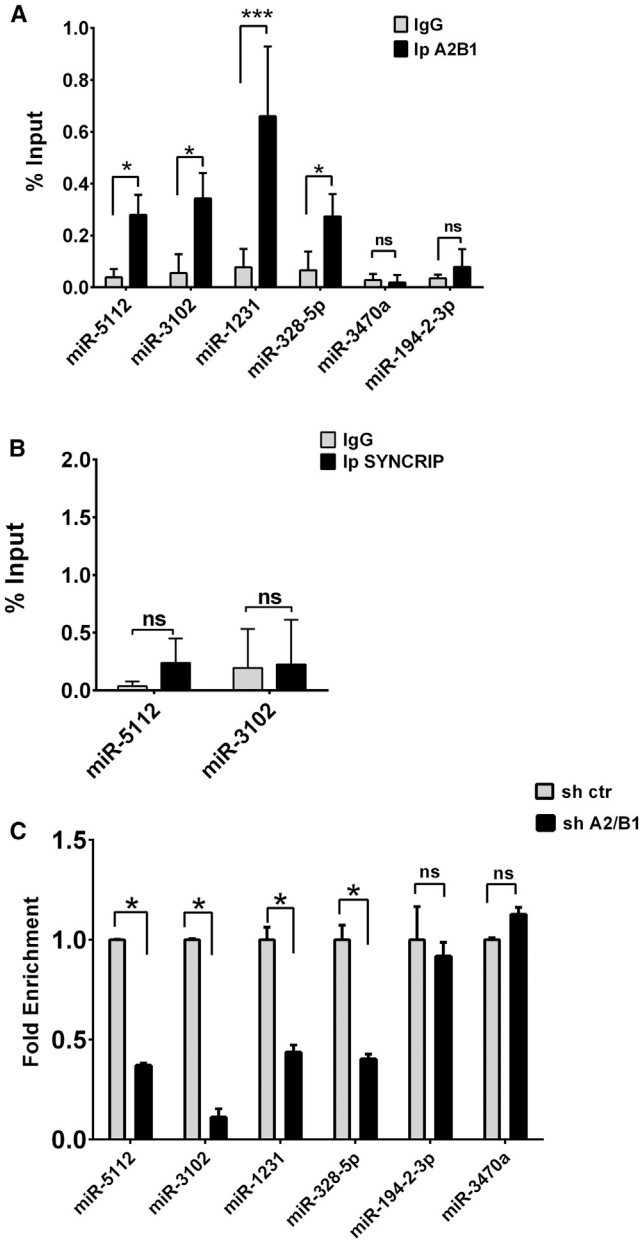

Figure 4. SYNCRIP and hnRNPA2B1 Display Different Sequence-Specific Exosomal Sorting Capacities

(A) RIP assays with goat polyclonal anti-hnRNPA2B1 and pre-immune IgG (as control) on murine hepatocyte cell extracts. miRNA levels in immunoprecipitated samples were determined by qRT-PCR and reported as percentage with respect to the input sample (% input). Data are means ± SD of three independent experiments, and statistically significant differences are reported (*$p < 0.05$; ***$p < 0.001$). See also Table S5.

(B) RIP assays with rabbit polyclonal anti-SYNCRIP and preimmune IgG (as control) on murine hepatocyte cell extracts. miRNA levels in immunoprecipitated samples were determined by qRT-PCR and reported as percentage with respect to the input sample (% input). Data are means ± SD of three independent experiments (ns, not statistically significant). See also Table S5.

(C) qRT-PCR analysis for the indicated miRNAs on hnRNPA2B1-silenced hepatocytes (shA2B1), compared to control shScramble cells (shCtr). The values are calculated by the ΔΔCt method, normalized to snRNA U6 levels, and shown as mean ± SD. Statistically significant differences are reported (*$p < 0.05$; ns, not significant) for three independent experiments. See also Figure S2D.

et al., 2005), selecting a minimum matrix similarity cutoff >0.60 (Table S5; Figure 3B). The consensus motif was computed, considering the weighted contribution of each nucleotide of the miRNA sequences and reporting the "core sequence" of the motif, defined as the four highest conserved positions and 1 nt up- and downstream of it, with a total length of 6 nt (Table S5; Figure 3B). Moreover, pull-down analysis highlighted that SYNCRIP-binding capacity is impaired when the GGCU sequence is mutated (Figure 3C).

In the light of these results, we hypothesized that the here-identified hEXO motif might have a functional role in exosomal miRNAs sorting. To gather evidence of the informational content of this motif, two pre-miRNAs were overexpressed; the first (i.e., miR-29b-3p) was an miRNA not embedding the hEXO motif and not efficiently bound to SYNCRIP in our in vitro pull-down assays (Figure 2A), and the second was an artificial miRNA derived from miR-29b that was engineered to embed the hEXO motif (hEXO-chimera-miR-29b) (Figure 3D). The cytoplasmic and exosomal contents of the respective mature wild-type (WT) miRNA-29b and the chimeric 23-mer were then assessed by qPCR by using specific primers (see Experimental Procedures). As shown in Figure 3E, the insertion of the hEXO sequence was sufficient to increase the exosome/cellular ratio; moreover the hEXO-chimera-miR-29b was found directly bound to SYNCRIP in RIP assays performed after UV cross-linking (Figure 3F).

Overall, these data indicate that a conserved sequence in the extra seed acts as an element influencing the exosomal compartmentalization of miRNAs and that the hnRNP SYNCRIP can differentially bind to miRNAs sharing this hEXO motif.

SYNCRIP and hnRNPA2B1 Display Different Sequence-Specific Exosomal Sorting Capacities

As mentioned above, a previous report identified in the sumoylated hnRNPA2B1-GGAG motif interaction a mechanism acting in lymphocytes for selective export of specific miRNAs (i.e., miRNA-198 and miRNA-601) (Villarroya-Beltri et al., 2013). Starting from the observation that the GGAG motif was found in a subset of hEXO miRNAs (13%; Table S5), with or without the hEXO motif GGCU, and from evidence indicating the sumoylation of SYNCRIP (Figures S2B and S2C), we aimed to assess whether hnRNPA2B1 might also have a role in hepatocytes, acting in a parallel, independent, or synergic mode with respect to SYNCRIP in the sorting of GGAG- or hEXO-motif-containing miRNAs.

The selective binding capacity of hnRNPA2B1 was assessed by RIP experiments after UV cross-linking; three miRNAs with the EXO motif (GGAG; Villarroya-Beltri et al., 2013) in their 3′end (i.e., miR-5112 and miR-3102-5p.2-5p and miR-1231; Table S4) and one (i.e., miR-328-5p) with both EXO and hEXO motifs (GGAG and GGCU, respectively) were enriched in hnRNPA2B1 immunoprecipitated samples (Figure 4A); notably, we observed no direct binding to the miR-3470a embedding only the hEXO motif. Similarly, SYNCRIP did not bind to miRNAs with only the GGAG EXO motif (i.e., miR-5112 and

miR-3102-5p.2-5p; Figure 4B). Moreover, knockdown of hnRNPA2B1 (Figure S2D) in hepatocytes did not caused a decrease in exosomal loading of GGCU-containing miR-3470a and miR-194-2-3p, while the number of miRNAs with the GGAG motif were reduced (Figure 4C).

Overall, although hnRNPs SYNCRIP and hnRNPA2B1 could interact within a common exosome-sorting complex, these data indicate that the two proteins display sequence-specific exosomal sorting capacity in the loading of selected miRNAs.

DISCUSSION

The main finding of this investigation is the identification of the RNA-interacting protein SYNCRIP as a component of the miRNA exosomal loading machinery, controlling the sorting of exosome-enriched miRNAs. SYNCRIP is a highly conserved RNA-binding protein identified in extracellular vesicles isolated from various cell types and annotated in the major exosome database (Keerthikumar et al., 2016). Several pieces of evidence point to a role for SYNCRIP in controlling RNA maturation and trafficking, including pre-mRNA splicing, RNA editing, cytoplasmic mRNA transport, internal ribosome entry site (IRES)-mediated translational activation, and mRNA degradation (Bannai et al., 2004; Blanc et al., 2001; Chen et al., 2008; Grosset et al., 2000; Kanai et al., 2004; Mourelatos et al., 2001). SYNCRIP is associated with multiprotein complexes, including the ApoB RNA editing complex and the survival of motor neuron (SMN) complex (Blanc et al., 2001), as well as with RNP granules containing mRNAs and non-coding regulatory RNAs (Bannai et al., 2004; Duning et al., 2008). Moreover, SYNCRIP was found in GW bodies (GWBs) containing the mRNA-binding protein GW182, a major player in RNA trafficking and storage (Moser et al., 2007), as well as in several membrane-trafficking proteins. Notably, SYNCRIP shows an RNA sequence/structure discriminatory capacity associated with (1) an RNA stem loop signal necessary to specifically localize an RNA transcript in the oocyte of *Drosophila*, where it influences vesicle release (Halstead et al., 2014; Van De Bor et al., 2005); and (2) specific viral transcripts, co-localizing with newly synthesized hepatitis C virus (HCV) RNA and enhancing HCV IRES-dependent translation (Cathariuss et al., 2005). Interestingly, the known functions of SYNCRIP also include the regulation of translation by competing with poly(A)-binding protein (PABP) (Svitkin et al., 2013).

Here, SYNCRIP was found to directly bind to some miRNAs enriched in exosomes sharing a short sequence (named the hEXO motif). The role of the hEXO motif in the regulation of exosomal miRNA localization was highlighted by its capacity to enhance the ability of an intracellular miRNA to be loaded into exosomes. While the hEXO motif differs from the previously identified AUAAUC SYNCRIP-binding motif (Chen et al., 2012), MatInspector analysis identifies the hEXO motif embedded in previously described SYNCRIP-binding sequences, i.e., nine times in the gurken transcript of *Drosophila* (McDermott et al., 2012), four times in the interleukin-8 (IL-8) mRNA 3′ UTR (Shimizu et al., 2014), and five times in HCV IRES (Kim et al., 2004).

Current knowledge concerning sequence elements controlling miRNA localization in exosome is limited to the evidence provided by Villaroja-Beltri and colleagues (Villarroya-Beltri et al., 2013), who identified in T cells a subset of miRNAs that share an EXO sequence motif (GGAG) able to control their loading into exosomes (Villarroya-Beltri et al., 2013). This sequence mediates binding to the sumoylated protein hnRNPA2B1, previously characterized for its activity in trafficking of other RNA species (reviewed in Villarroya-Beltri et al., 2014). While this first piece of evidence demonstrated that specific proteins may govern miRNA sorting by recognizing and binding to specific sequences in the RNAs, it is conceivable that a loading ribonucleoprotein machinery might involve several molecular players, each governing exosomal sorting of a specific class of miRNAs.

Here, evidence based on the biochemical analyses we performed indicates that each protein directly binds to a specific sequence and that some miRNAs embed both EXO and hEXO motifs.

Although our evidence indicating the sumoylation of SYNCRIP is provocative in that it suggests this post translational modification (PTM) is a common feature of components of the exosomal loading machinery, further studies are needed to demonstrate a functional requirement for sumoylation.

This study has contributed to shed light on hepatocytes vesicle-associated miRNA secretome, which might have a tissue-specific profile. These findings open the way for the possible selective modification of the miRNA exosomal cargo that, in turn, may impact cell-to-cell communication for a broad spectrum of applications. Further studies are now required to approach the systematic characterization of the ribonuclear machinery, which might include tissue-specific cellular factors, that governs the exosome-mediated pivotal mechanism of cell-to-cell communication.

EXPERIMENTAL PROCEDURES

Cell Culture Conditions

Nontumorigenic murine hepatocyte 3A cells (Conigliaro et al., 2013) were grown in RPMI 1640 medium supplemented with 10% FBS (Gibco Life Technology), 50 ng/mL epidermal growth factor (EGF), 30 ng/mL insulin growth factor (IGF) II (PeproTech), 10 μg/mL insulin (Roche), and penicillin/streptomycin, on dishes coated with collagen I (Gibco Life Technology). To collect hepatocyte exosomes, 80 × 10^6 cells were cultured for 72 hr in RPMI-1640 supplemented with 10% FBS depleted of bovine exosomes by overnight centrifugation at 100,000 × *g* (Beckman Optima L80; Beckman Coulter).

Exosome Purification

Extracellular vesicles were prepared according to International Society of Extracellular Vesicles (ISEV) recommendations. In brief, to isolate exosomes, conditioned media (CM) from 12 150 mm plates each containing 13 million hepatocytes was collected after 72-hr culture in complete medium containing exo-depleted FBS. Cell-conditioned media was centrifuged at 300 × *g* for 10 min to remove cells and then at 2,000 × *g* for 20 min and 16,000 × *g* for 1 hr to remove cell debris. Cleared supernatants were passed through 0.22 μm filter membranes, concentrated by an Amicon Ultra-15 centrifugal filter device (Merck Millipore), ultracentrifuged in a SW28 rotor at 100,000 rpm for 70 min, and finally resuspended in PBS.

Exosome Fractionation

To separate vesicles from large protein complexes the exosome suspension was subjected to SEC and fractionated with Exo-spin midi-columns (CELL Guidance Systems) according to the manufacturer's instructions. Briefly, exosomes were precipitated with Buffer A overnight at 4°C and the exosome-containing pellet was suspended in 1 mL PBS. Subsequently, the exosome suspension was applied in 500-μL increments to the top of the column,

previously equilibrated with PBS, to collect the initial two fractions, and the other 13 fractions were collected by adding 500 μL PBS 13 times. Most of the exosomes were eluted between fractions 7 and 10. The exosome-containing fractions were precipitated again with buffer A overnight at 4°C and then lysed for western blotting experiment. Proteins were quantified by Bradford protein assay reagent (Bio-Rad), separated by SDS-PAGE, and transferred onto nitrocellulose membranes (Hybond ECLTM, GE Healthcare). Blots were blocked in 5% non-fat milk prepared in TBST and incubated overnight at 4°C with the primary antibodies. The following primary antibodies were used: mouse anti-Tsg101 (clone C-2, Santa Cruz Biotechnology), mouse anti-Alix (Cell Signaling Technology), and mouse anti-hnRNPQ antibody (clone 7A11.2, EMD Millipore, Merck). Blots were incubated with HRP-conjugated anti-mouse secondary antibody (170-6516, Bio-Rad) followed by enhanced chemiluminescence reaction (WESTAR NOVA 2011 or ηC, Cyanagen).

500-μL fractions were collected and their characterization performed by western blot analysis of known exosomal markers (i.e., Alix and Tsg101). Exosome size was determined by nanoparticle tracking analysis with Nanosight LM-10 (Malvern Instruments). To remove contaminant non-vesicular RNA-proteins (Hill et al., 2013), exosomes were treated with 100 μg/mL proteinase K (60 min) followed by heat inactivation of the protease; unprotected RNA was degraded by 15-min incubation with 2 μg/mL protease-free RNase A (Sigma-Aldrich) followed by addition of RNAsin RNase inhibitor (Promega). To assess intravesicular localization of SYNCRIP, extracellular vesicle suspensions were treated with 100 μg/mL proteinase K alone or with a combination of both proteinase K and 0.5% Triton X-100 at 37°C for 60 min and then analyzed by western blot.

Biotin miRNA Pull-Down

Biotin miRNA pull-down experiments were performed on cytoplasmic extracts. Briefly, cells were lysed in hypotonic buffer (10 mM Tris-Cl [pH 7.5], 20 mM KCl, 1.5 mM $MgCl_2$, 5 mM DTT, 0.5 mM EGTA, 5% glycerol, 0.5% NP-40, and 40 U/μL Rnasin [Promega]) supplemented with protease inhibitors (Roche Applied Science). After centrifugation at 2,000 × *g* to remove nuclei, cytoplasmic extracts were clarified at 10,000 at 4°C for 10 min and incubated for 1 hr at 4°C with 10 nmol synthetic single strand miRNA oligonucleotides containing a biotin modification attached to the 5′ end via a spacer arm (Sigma-Aldrich) (Figures 2 and 3, legends; Table S6A; Heo et al., 2009). SoftLink Soft Release Avidin Resin beads, previously blocked with 1 μg/μL yeast tRNA (Roche Applied Science), were added to reaction mixture for 90 min at 4°C, and then the beads were washed five times with 1 mL lysis buffer and once with PBS. Elution was for 1 hr at room temperature with 5 mM biotin to allow collection of bound proteins (Martin et al., 2014). MS analysis is detailed in the Supplemental Experimental Procedures.

RNA Extraction and RNA Quality Control

Total RNA from cells and exosomes was isolated by Qiazol and the miRNeasy Mini Kit (QIAGEN) following the manufacturer's protocols. RNA purity was assessed by spectrophotometric measure of optical density 260 (OD_{260})/OD_{280} ~2 and OD_{260}/OD_{230} >1.8 with a Nanodrop 2000c Spectrophotometer (Thermo Fisher Scientific), and RNA quantitation was performed with Qubit and a Qubit RNA assay (Life Technologies). For miRNA-seq experiments, the quality of isolated RNA was determined with Bioanalyzer 2100 (Agilent Technologies).

Small RNA Sequencing

RNA samples were purified from several independent cell cultures and exosome isolates and then pooled together. Indexed libraries were prepared from ~500 ng/ea (each) purified RNA pool with a TruSeq Small RNA Sample Prep Kit (Illumina), as described previously (Nassa et al., 2014). Then, miRNA expression profiles were analyzed by small RNA-seq. Size-indexed miRNA libraries were gel purified and sequenced in triplicate on a HiSeq2500 (Illumina) at a concentration of 10 pM per lane for 50 cycles plus seven additional cycles for index sequencing.

Mapping of Small RNA Reads

Read sequence quality checks were performed by FastQC (Babraham Bioinformatics; http://www.bioinformatics.babraham.ac.uk/projects/fastqc/). Data analysis was performed using iMir pipeline and applying the standard workflow, using miRBase version 20 as a reference track to identify mature miRNAs (Giurato et al., 2013). To increase specificity in miRNA identification, reads alignment was performed with zero mismatches; moreover, miRNAs were considered to be expressed when they were detected by at least the value of the first quantile of the considered dataset or replicate. Raw miRNA sequencing data have been deposited in the database: EBI ArrayExpress (http://www.ebi.ac.uk/arrayexpress) according to the Minimum Information about high-throughput SEQuencing Experiment (MINSEQE) guidelines (accession number: E-MTAB-4502). Differential expression analysis was performed with DESeq2 (Love et al., 2014), and only miRNAs showing fold change ≤ -1.5 and ≥ 1.5, with FDR ≤ 0.10, were considered to be differentially expressed.

Over-Represented Motif Analysis

An unbiased search to identify over-represented motifs on exosome-enriched miRNAs was performed using Improbizer (Ao et al., 2004). A zero-or-one occurrence model was used to find over-represented 4- to 8-nt-long motifs. The remaining miRNAs annotated in miRBase v20 were used as background. A Markov model of order 0 was assumed for the background sequences. Improbizer results were replicated using MatDefine (Genomatix) (Cartharius et al., 2005) setting a matrix similarity >0.60. MatInspector (Genomatix) was used to search for motifs in miRNAs sequences.

RT-PCR and Real-Time PCR

Intracellular and exosomal total RNA (50–100 ng) was reverse transcribed with the miScript II Reverse Transcriptase Kit (QIAGEN) according to the manufacturer's protocol. Diluted (1:20) cDNA samples were used for qPCR in a total volume of 20 μL using the miScript SYBR Green PCR Kit and miRNA-specific primers (QIAGEN). Relative amounts of intracellular miRNAs were obtained using the $2^{-\Delta\Delta Ct}$ method (Livak and Schmittgen, 2001). The small RNA U6 was used for normalization of miRNA relative quantities in both cellular and exosomal preparations.

qRT-PCR was performed with CFX Connect, and data analysis was performed using CFX Manager Software (Bio-Rad).

RIP and UV Cross-Linking RIP

Cells were lysed in ice-cold lysis buffer (10 mM HEPES [pH 7.3], 50 mM KCl, 0.5% NP-40, 5 mM $MgCl_2$, and 0.5 mM DTT) supplemented with protease inhibitors (Roche Applied Science), recombinant RNase inhibitors (Promega), and 1 mM PMSF. The lysates were centrifuged for 15 min at 12,000 × *g*, and 50 μL was saved as input. 1 mg protein extract was incubated with 3 μg rabbit anti-hnRNPQ antibody (Medical & Biological Laboratories) or mock antibody (rabbit immunoglobulin G [IgG], EMD Millipore) for 2 hr at 4°C with end-over-end rotation. 30 μL protein G Dynabeads (Invitrogen), blocked with 1 μg/μL yeast tRNA (Roche Applied Science), was added for 1 hr, followed by five washes with ice-cold lysis buffer.

Coimmunoprecipitated miRNAs were extracted using Qiazol and the miRNeasy kit (QIAGEN). qPCR analysis was performed with SYBR green qPCR (QIAGEN), and miRNA fold enrichment in immunoprecipitated samples was expressed as percent input (one-tenth of cell lysate) and compared to IgG isotypic control.

In UV cross-linking RIP, hepatocytes were washed twice with PBS and subjected to UV cross-linking (one time irradiation at 800 mJ/cm^2 in 254 nm Stratalinker [Stratagene 2400, Stratagene]). Cells were then lysed in 10 mM HEPES (pH 7.3), 20 mM KCl, 2 mM $MgCl_2$, 0.5 mM EGTA, 1 mM EDTA, 1 mM DTT, 40 U/μL RNAsin inhibitor, 0.1% SDS, 0.5% sodium deoxycholate, and 0.5% NP40. Endogenous SYNCRIP was immunoprecipitated with rabbit anti-hnRNPQ antibody (Medical & Biological Laboratories) and incubated with protein G Dynabeads (Invitrogen) for 1 hr. Denaturing washes were performed as described previously (McHugh et al., 2015; Battistelli et al., 2016) to allow only the detection of direct interactions. Coimmunoprecipitated miRNAs were extracted using Qiazol and the miRNeasy kit. qPCR analysis was performed with SYBR green qPCR (QIAGEN) and miRNA fold enrichment in immunoprecipitated samples were expressed as percent input and compared to IgG isotypic control.

shRNA Silencing

Stable SYNCRIP and hnRNPA2B1 knockdowns were achieved through infection with shRNAs cloned in pSUPER retro puro retroviral vector (Oligoengine). Viral supernatants were collected 48 hr after transfection of 293 gp packaging cells, filtered (0.45 μm), and added to hepatocytes. At 48 hr post-infection, selection was performed with 1.5 μg/mL puromycin for at least 1 week before analysis. The sequences of shRNA oligos used for cloning are reported in Table S6. The sequence of shRNA scramble used as control was previously described (Pasque et al., 2011).

Cloning of miR-29b-3p and hEXO Chimera mR-29b and Lentiviral Transduction

Artificial introns carrying the synthetic stem-loop precursors of miR-29b-3p and hEXO chimera miR-29b (GeneArt Gene Synthesis, Life Technologies) were cloned in pLENTI 7.3/V5-DEST lentiviral vector. HEK293T cells were co-transfected using Fugene HD (Promega) with an miRNA-encoding vector and packaging empty plasmids pLP1, pLP2, and pLP/VSV-G (Thermo Fisher Scientific). Supernatants were collected after 48 hr, filtered (0.45 μm), and added to hepatocytes.

Statistical Analyses

For small RNA-seq studies, the experiment was performed using three biological replicates. miRNAs were considered to be expressed when they were detected with an expression value above the first quantile of the expression distribution levels for the considered dataset/replicate. PCA and Poisson distance were used to determine how miRNA profiles differ between cells and exosomes. Differentially enriched miRNAs between cells and exosomes were computed using DESeq2 (Love et al., 2014), considering an FE cutoff ≥ 1.5 (or ≤ -1.5) and a FDR ≤ 0.10. For motif analysis, a Markov model of order 0 was used in Improbizer (Ao et al., 2004), while a matrix similarity >0.60 was used in MatDefine (Genomatix). In heatmap representations, expression values were indicated in RPM (log2 scale). For the qRT-PCR analysis, statistical differences were assessed with the one-tailed paired Student's t-test using GraphPad Prism Version 6 (GraphPad Software). Data are presented as mean ± SD, and p values < 0.05 were considered statistically significant.

ACCESSION NUMBERS

The accession number for the raw miRNA sequencing data reported in this paper is EBI: E-MTAB-4502.

SUPPLEMENTAL INFORMATION

Supplemental Information includes Supplemental Experimental Procedures, two figures, and six tables and can be found with this article online at http://dx.doi.org/10.1016/j.celrep.2016.09.031.

AUTHOR CONTRIBUTIONS

L.S. participated to the experimental design and the interpretation of results, performed cellular and molecular analysis, and contributed to manuscript writing. G.G., R.T., and A.W. performed next-generation sequencing and bioinformatics analyses and contributed to experimental planning and manuscript writing. C.C. participated in research planning and coordination of the experimental work, interpreted the results, and wrote the manuscript. C. Montaldo and C. Mancone performed proteomic experiments. C.B. conducted molecular experiments. T.A. contributed to critical revisions. M.T. designed the research plan, coordinated the experimental work, interpreted the results, and wrote the manuscript.

ACKNOWLEDGMENTS

This work was supported by Associazione Italiana per la Ricerca sul Cancro (AIRC; grants IG-14114 and IG-17426), the Ministry for Health of Italy (Ricerca Corrente to M.T., T.A., C. Montaldo, and L.S.), Ministero Università e Ricerca Scientifica (grants PRIN 2010LC747T and FIRB RBFR12W5V5_003), Consiglio Nazionale delle Ricerche (CNR; Flagship Project InterOmics), and Genomix4Life Srl. L.S. was the recipient of a Fondazione Umberto Veronesi postdoctoral fellowship (2014).

Received: April 12, 2016
Revised: July 6, 2016
Accepted: September 9, 2016
Published: October 11, 2016

REFERENCES

Ao, W., Gaudet, J., Kent, W.J., Muttumu, S., and Mango, S.E. (2004). Environmentally induced foregut remodeling by PHA-4/FoxA and DAF-12/NHR. Science *305*, 1743–1746.

Bannai, H., Fukatsu, K., Mizutani, A., Natsume, T., Iemura, S., Ikegami, T., Inoue, T., and Mikoshiba, K. (2004). An RNA-interacting protein, SYNCRIP (heterogeneous nuclear ribonuclear protein Q1/NSAP1) is a component of mRNA granule transported with inositol 1,4,5-trisphosphate receptor type 1 mRNA in neuronal dendrites. J. Biol. Chem. *279*, 53427–53434.

Battistelli, C., Cicchini, C., Santangelo, L., Tramontano, A., Grassi, L., Gonzalez, F.J., de Nonno, V., Grassi, G., Amicone, L., and Tripodi, M. (2016). The Snail repressor recruits EZH2 to specific genomic sites through the enrollment of the lncRNA HOTAIR in epithelial-to-mesenchymal transition. Oncogene, Published online July 25, 2016. http://dx.doi.org/10.1038/onc.2016.260.

Blanc, V., Navaratnam, N., Henderson, J.O., Anant, S., Kennedy, S., Jarmuz, A., Scott, J., and Davidson, N.O. (2001). Identification of GRY-RBP as an apolipoprotein B RNA-binding protein that interacts with both apobec-1 and apobec-1 complementation factor to modulate C to U editing. J. Biol. Chem. *276*, 10272–10283.

Cartharius, K., Frech, K., Grote, K., Klocke, B., Haltmeier, M., Klingenhoff, A., Frisch, M., Bayerlein, M., and Werner, T. (2005). MatInspector and beyond: promoter analysis based on transcription factor binding sites. Bioinformatics *21*, 2933–2942.

Cha, D.J., Franklin, J.L., Dou, Y., Liu, Q., Higginbotham, J.N., Demory Beckler, M., Weaver, A.M., Vickers, K., Prasad, N., Levy, S., et al. (2015). KRAS-dependent sorting of miRNA to exosomes. eLife *4*, e07197.

Chen, H.H., Chang, J.G., Lu, R.M., Peng, T.Y., and Tarn, W.Y. (2008). The RNA binding protein hnRNP Q modulates the utilization of exon 7 in the survival motor neuron 2 (SMN2) gene. Mol. Cell. Biol. *28*, 6929–6938.

Chen, H.H., Yu, H.I., Chiang, W.C., Lin, Y.D., Shia, B.C., and Tarn, W.Y. (2012). hnRNP Q regulates Cdc42-mediated neuronal morphogenesis. Mol. Cell. Biol. *32*, 2224–2238.

Conigliaro, A., Amicone, L., Costa, V., De Santis Puzzonia, M., Mancone, C., Sacchetti, B., Cicchini, C., Garibaldi, F., Brenner, D.A., Kisseleva, T., et al. (2013). Evidence for a common progenitor of epithelial and mesenchymal components of the liver. Cell Death Differ. *20*, 1116–1123.

De Toro, J., Herschlik, L., Waldner, C., and Mongini, C. (2015). Emerging roles of exosomes in normal and pathological conditions: new insights for diagnosis and therapeutic applications. Front. Immunol. *6*, 203.

Duning, K., Buck, F., Barnekow, A., and Kremerskothen, J. (2008). SYNCRIP, a component of dendritically localized mRNPs, binds to the translation regulator BC200 RNA. J. Neurochem. *105*, 351–359.

Giurato, G., De Filippo, M.R., Rinaldi, A., Hashim, A., Nassa, G., Ravo, M., Rizzo, F., Tarallo, R., and Weisz, A. (2013). iMir: an integrated pipeline for high-throughput analysis of small non-coding RNA data obtained by smallRNA-Seq. BMC Bioinformatics *14*, 362.

Grosset, C., Chen, C.Y., Xu, N., Sonenberg, N., Jacquemin-Sablon, H., and Shyu, A.B. (2000). A mechanism for translationally coupled mRNA turnover: interaction between the poly(A) tail and a c-fos RNA coding determinant via a protein complex. Cell *103*, 29–40.

Guduric-Fuchs, J., O'Connor, A., Camp, B., O'Neill, C.L., Medina, R.J., and Simpson, D.A. (2012). Selective extracellular vesicle-mediated export of

an overlapping set of microRNAs from multiple cell types. BMC Genomics *13*, 357.

Guo, L., and Guo, N. (2015). Exosomes: Potent regulators of tumor malignancy and potential bio-tools in clinical application. Crit. Rev. Oncol. Hematol. *95*, 346–358.

Halstead, J.M., Lin, Y.Q., Durraine, L., Hamilton, R.S., Ball, G., Neely, G.G., Bellen, H.J., and Davis, I. (2014). Syncrip/hnRNP Q influences synaptic transmission and regulates BMP signaling at the Drosophila neuromuscular synapse. Biol. Open *3*, 839–849.

Heo, I., Joo, C., Kim, Y.K., Ha, M., Yoon, M.J., Cho, J., Yeom, K.H., Han, J., and Kim, V.N. (2009). TUT4 in concert with Lin28 suppresses microRNA biogenesis through pre-microRNA uridylation. Cell *138*, 696–708.

Hill, A.F., Pegtel, D.M., Lambertz, U., Leonardi, T., O'Driscoll, L., Pluchino, S., Ter-Ovanesyan, D., and Nolte-'t Hoen, E.N. (2013). ISEV position paper: extracellular vesicle RNA analysis and bioinformatics. J. Extracell. Vesicles *2*, 2.

Huang, X., Yuan, T., Tschannen, M., Sun, Z., Jacob, H., Du, M., Liang, M., Dittmar, R.L., Liu, Y., Liang, M., et al. (2013). Characterization of human plasma-derived exosomal RNAs by deep sequencing. BMC Genomics *14*, 319.

Janas, T., Janas, M.M., Sapoń, K., and Janas, T. (2015). Mechanisms of RNA loading into exosomes. FEBS Lett. *589*, 1391–1398.

Kanai, Y., Dohmae, N., and Hirokawa, N. (2004). Kinesin transports RNA: isolation and characterization of an RNA-transporting granule. Neuron *43*, 513–525.

Keerthikumar, S., Chisanga, D., Ariyaratne, D., Al Saffar, H., Anand, S., Zhao, K., Samuel, M., Pathan, M., Jois, M., Chilamkurti, N., et al. (2016). ExoCarta: a web-based compendium of exosomal cargo. J. Mol. Biol. *428*, 688–692.

Kim, J.H., Paek, K.Y., Ha, S.H., Cho, S., Choi, K., Kim, C.S., Ryu, S.H., and Jang, S.K. (2004). A cellular RNA-binding protein enhances internal ribosomal entry site-dependent translation through an interaction downstream of the hepatitis C virus polyprotein initiation codon. Mol. Cell. Biol. *24*, 7878–7890.

Koppers-Lalic, D., Hackenberg, M., Bijnsdorp, I.V., van Eijndhoven, M.A., Sadek, P., Sie, D., Zini, N., Middeldorp, J.M., Ylstra, B., de Menezes, R.X., et al. (2014). Nontemplated nucleotide additions distinguish the small RNA composition in cells from exosomes. Cell Rep. *8*, 1649–1658.

Liu, H.M., Aizaki, H., Choi, K.S., Machida, K., Ou, J.J., and Lai, M.M. (2009). SYNCRIP (synaptotagmin-binding, cytoplasmic RNA-interacting protein) is a host factor involved in hepatitis C virus RNA replication. Virology *386*, 249–256.

Livak, K.J., and Schmittgen, T.D. (2001). Analysis of relative gene expression data using real-time quantitative PCR and the 2(-Delta Delta C(T)) Method. Methods *25*, 402–408.

Lo Cicero, A., Stahl, P.D., and Raposo, G. (2015). Extracellular vesicles shuffling intercellular messages: for good or for bad. Curr. Opin. Cell Biol. *35*, 69–77.

Love, M.I., Huber, W., and Anders, S. (2014). Moderated estimation of fold change and dispersion for RNA-seq data with DESeq2. Genome Biol. *15*, 550.

Martin, H.C., Wani, S., Steptoe, A.L., Krishnan, K., Nones, K., Nourbakhsh, E., Vlassov, A., Grimmond, S.M., and Cloonan, N. (2014). Imperfect centered miRNA binding sites are common and can mediate repression of target mRNAs. Genome Biol. *15*, R51.

McDermott, S.M., Meignin, C., Rappsilber, J., and Davis, I. (2012). Drosophila Syncrip binds the gurken mRNA localisation signal and regulates localised transcripts during axis specification. Biol. Open *1*, 488–497.

McHugh, C.A., Chen, C.K., Chow, A., Surka, C.F., Tran, C., McDonel, P., Pandya-Jones, A., Blanco, M., Burghard, C., Moradian, A., et al. (2015). The Xist lncRNA interacts directly with SHARP to silence transcription through HDAC3. Nature *521*, 232–236.

Mittelbrunn, M., and Sánchez-Madrid, F. (2012). Intercellular communication: diverse structures for exchange of genetic information. Nat. Rev. Mol. Cell Biol. *13*, 328–335.

Mittelbrunn, M., Gutiérrez-Vázquez, C., Villarroya-Beltri, C., González, S., Sánchez-Cabo, F., González, M.A., Bernad, A., and Sánchez-Madrid, F. (2011). Unidirectional transfer of microRNA-loaded exosomes from T cells to antigen-presenting cells. Nat. Commun. *2*, 282.

Moser, J.J., Eystathioy, T., Chan, E.K., and Fritzler, M.J. (2007). Markers of mRNA stabilization and degradation, and RNAi within astrocytoma GW bodies. J. Neurosci. Res. *85*, 3619–3631.

Mourelatos, Z., Abel, L., Yong, J., Kataoka, N., and Dreyfuss, G. (2001). SMN interacts with a novel family of hnRNP and spliceosomal proteins. EMBO J. *20*, 5443–5452.

Nassa, G., Tarallo, R., Giurato, G., De Filippo, M.R., Ravo, M., Rizzo, F., Stellato, C., Ambrosino, C., Baumann, M., Lietzèn, N., et al. (2014). Post-transcriptional regulation of human breast cancer cell proteome by unliganded estrogen receptor β via microRNAs. Mol. Cell. Proteomics *13*, 1076–1090.

Nolte-'t Hoen, E.N., Buermans, H.P., Waasdorp, M., Stoorvogel, W., Wauben, M.H., and 't Hoen, P.A. (2012). Deep sequencing of RNA from immune cell-derived vesicles uncovers the selective incorporation of small non-coding RNA biotypes with potential regulatory functions. Nucleic Acids Res. *40*, 9272–9285.

Ohshima, K., Inoue, K., Fujiwara, A., Hatakeyama, K., Kanto, K., Watanabe, Y., Muramatsu, K., Fukuda, Y., Ogura, S., Yamaguchi, K., and Mochizuki, T. (2010). Let-7 microRNA family is selectively secreted into the extracellular environment via exosomes in a metastatic gastric cancer cell line. PLoS ONE *5*, e13247.

Pasque, V., Gillich, A., Garrett, N., and Gurdon, J.B. (2011). Histone variant macroH2A confers resistance to nuclear reprogramming. EMBO J. *30*, 2373–2387.

Shimizu, Y., Nishitsuji, H., Marusawa, H., Ujino, S., Takaku, H., and Shimotohno, K. (2014). The RNA-editing enzyme APOBEC1 requires heterogeneous nuclear ribonucleoprotein Q isoform 6 for efficient interaction with interleukin-8 mRNA. J. Biol. Chem. *289*, 26226–26238.

Skog, J., Würdinger, T., van Rijn, S., Meijer, D.H., Gainche, L., Sena-Esteves, M., Curry, W.T., Jr., Carter, B.S., Krichevsky, A.M., and Breakefield, X.O. (2008). Glioblastoma microvesicles transport RNA and proteins that promote tumour growth and provide diagnostic biomarkers. Nat. Cell Biol. *10*, 1470–1476.

Svitkin, Y.V., Yanagiya, A., Karetnikov, A.E., Alain, T., Fabian, M.R., Khoutorsky, A., Perreault, S., Topisirovic, I., and Sonenberg, N. (2013). Control of translation and miRNA-dependent repression by a novel poly(A) binding protein, hnRNP-Q. PLoS Biol. *11*, e1001564.

Van De Bor, V., Hartswood, E., Jones, C., Finnegan, D., and Davis, I. (2005). gurken and the I factor retrotransposon RNAs share common localization signals and machinery. Dev. Cell *9*, 51–62.

Villarroya-Beltri, C., Gutiérrez-Vázquez, C., Sánchez-Cabo, F., Pérez-Hernández, D., Vázquez, J., Martin-Cofreces, N., Martinez-Herrera, D.J., Pascual-Montano, A., Mittelbrunn, M., and Sánchez-Madrid, F. (2013). Sumoylated hnRNPA2B1 controls the sorting of miRNAs into exosomes through binding to specific motifs. Nat. Commun. *4*, 2980.

Villarroya-Beltri, C., Baixauli, F., Gutiérrez-Vázquez, C., Sánchez-Madrid, F., and Mittelbrunn, M. (2014). Sorting it out: regulation of exosome loading. Semin. Cancer Biol. *28*, 3–13.

Vlassov, A.V., Magdaleno, S., Setterquist, R., and Conrad, R. (2012). Exosomes: current knowledge of their composition, biological functions, and diagnostic and therapeutic potentials. Biochim. Biophys. Acta *1820*, 940–948.

Zhang, J., Li, S., Li, L., Li, M., Guo, C., Yao, J., and Mi, S. (2015). Exosome and exosomal microRNA: trafficking, sorting, and function. Genomics Proteomics Bioinformatics *13*, 17–24.